PHYSICAL REVIEW
LETTERS

VOLUME 80 | 13 APRIL 1998 | NUMBER 15

Observation of Scalar Aharonov-Bohm Effect with Longitudinally Polarized Neutrons

W.-T. Lee,[1] O. Motrunich,[2] B. E. Allman,[3] and S. A. Werner[1]
[1]*Department of Physics and Astronomy and Research Reactor Center, University of Missouri–Columbia, Columbia, Missouri 65211*
[2]*Physics Department, Princeton University, Princeton, New Jersey 08544*
[3]*School of Physics, University of Melbourne, Parkville, 3052 Australia*
(Received 7 November 1997)

We have carried out a neutron interferometry experiment using longitudinally polarized neutrons to observe the scalar Aharonov-Bohm effect. The neutrons inside the interferometer are polarized parallel to an applied pulsed magnetic field $\mathbf{B}(t)$. The pulsed $\mathbf{B}$ field is spatially uniform so it exerts no force on the neutrons. Its direction also precludes the presence of any classical torque to change the neutron polarization. [S0031-9007(98)05764-0]

PACS numbers: 03.65.Bz, 42.50.–p

One distinction that sets quantum mechanics apart from classical mechanics is the treatment of a potential. In classical mechanics, the presence of a potential can be inferred only from the motion of the particles under the influence of the force it generates. The motion of particles through a region of uniform potential is, therefore, no different from that in empty space. In quantum mechanics, however, particles passing through a potential, uniform or not, acquire a quantum mechanical phase shift through their interaction with the potential. For instance, the phase shift acquired by electrons passing through a region of space containing a magnetic vector potential $\mathbf{A}$ and a scalar electric potential V is given by the action integral

$$\Delta\Phi = \frac{1}{\hbar}\left[\int\left(m\mathbf{v} + \frac{e}{c}\mathbf{A}\right)\cdot d\mathbf{r} - \int eV(t)\,dt\right]. \quad (1)$$

This phase shift can be detected by interferometric techniques, as first pointed out clearly by Aharonov and Bohm (AB) [1]. The vector AB effect arises from the vector potential $\mathbf{A}(\mathbf{r})$ in the spatial part of the action integral, while the scalar AB effect comes from the potential $V(t)$ in the temporal part. However, the experimental realization of the scalar Aharonov-Bohm (SAB) effect has proven to be challenging due to the technical difficulties in electron interferometry. The forces acting on the electrons render the experiment by Mateucci and Pozzi [2] inconclusive. A SAB neutron interferometry experiment, the analog of the electron experimental idea, was first suggested by Zeilinger [3] and later by Anandan [4], and subsequently carried out by Allman *et al.* using unpolarized incident neutron [5]. In this experiment, the magnetic moments μ of unpolarized thermal neutrons were subjected to a spatially uniform, but time-dependent magnetic induction $\mathbf{B}(t) = B(t)\hat{\mathbf{x}}$. The scalar interaction $E = -\boldsymbol{\mu}\cdot\mathbf{B}(t)$ produces a quantum mechanical phase shift that is measurable by neutron interferometry. In this experiment, a spin-independent phase shifter was used to establish separate control over the phase shifts for the spin-up and the spin-down neutron states. However, the use of unpolarized neutrons gave rise to the interpretational objection that each neutron experiences a classical torque [6], $\boldsymbol{\tau} = \boldsymbol{\mu}\times\mathbf{B}(t)$, and, therefore, the observed phase shift is not strictly SAB, but an effect also observable by classical polarimetry [7]. We have now carried out a similar SAB experiment, but using neutrons polarized along the $\mathbf{B}(t)$ field. In this arrangement, there is neither a classical torque nor (as before) a classical force exerted on the neutrons.

The experimental setup is shown schematically in Fig. 1. The setup consists of two main parts: the neutron polarizer and the neutron interferometer. The neutron polarizer includes a double-bounce neutron reflector made from a perfect silicon crystal and a magnetic prism assembly. The principle behind the polarizer is birefringence; i.e., the polarization dependence of the neutron

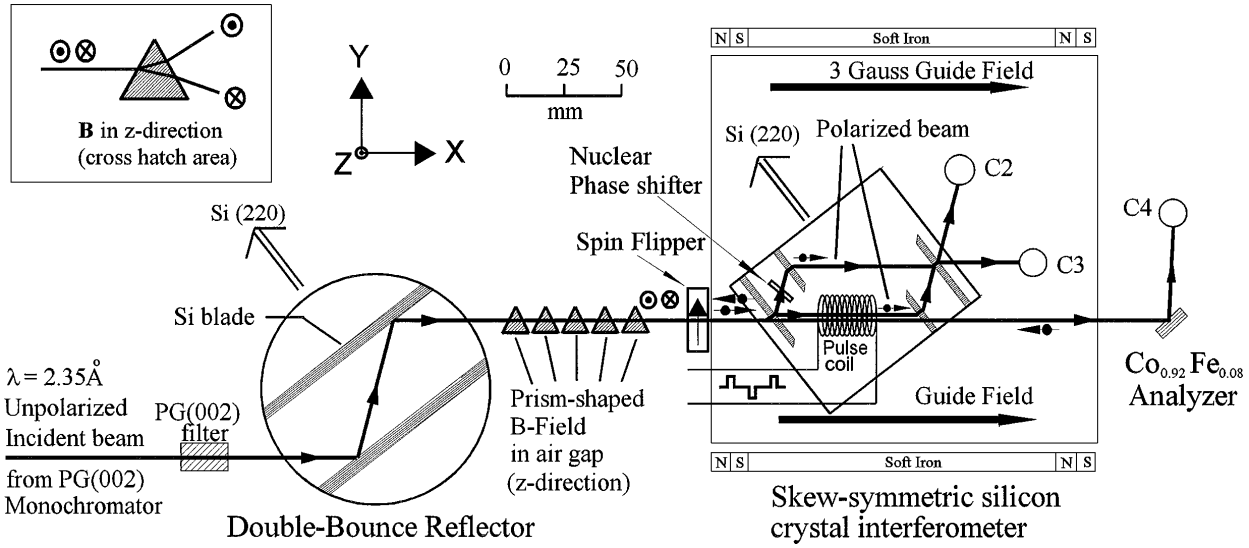

FIG. 1. Schematic drawing of the experimental setup. The polarizer consists of the perfect silicon crystal double-bounce reflector and the series of five prism-shaped air-gap magnetic fields. The silicon skew-symmetric interferometer and the pulse coil are the key components to observe the SAB effect. A static type spin flipper is placed between the polarizer and the interferometer to rotate the neutron spins from the z direction to the longitudinal x direction. The permanent magnet guide field maintains this direction of polarization throughout the region of the interferometer. Behind the interferometer is a magnetically saturated $Co_{0.92}Fe_{0.08}(111)$ crystal to analyze the classical spin orientation.

index of refraction [8]. As illustrated in Fig. 1, monochromatic neutrons with *nominal* wavelength 2.35 Å from a 0.4° mosaic PG(002) vertically focusing monochromator are incident upon the double-bounce crystal, which is machined so that the (220) reciprocal lattice vector is perpendicular to the crystal surfaces. The neutrons that satisfy the Bragg condition $\lambda = 2d \sin\theta_B$ for the Si(220) lattice planes to within the Darwin width $\Delta\theta_D = 1.6$ arcsec are reflected from the two blades of the double-bounce neutron reflector. The selected neutrons then travel through the air gap within each of five pairs of prism-shaped NdFeB magnets, producing uniform magnetic fields $\mathbf{B} = B(x, y)\hat{\mathbf{z}}$ of 8 kG. The interaction of the neutron with the magnetic field leads to two indices of refraction for the neutron spin states $\sigma = \pm 1$. Coupled with the boundary condition of the neutron wave function entering and leaving the region of the magnetic field, the prism field acts to refract the two spin states into two slightly diverging directions (inset of Fig. 1).

The monolithic, perfect silicon crystal skew-symmetric interferometer [9] downstream also uses the Si(220) reflection, but in Laue geometry, and also has an angular acceptance equal to the Darwin width. By rotating the double-bounce reflector against the interferometer, one of the two polarized neutron beam states can be aligned to satisfy the Bragg reflection condition of the interferometer, while the other polarization state passes through the interferometer without being reflected. A rocking curve of the double-bounce reflector against the interferometer showing the birefringence splitting of the neutron beam into two polarized beams is shown in Fig. 2. A double Gaussian curve fit gives a 3.3 arcsec separation in agreement with a calculation. In the experiment, we align the instrument at the center of one of the two peaks. The polarized neutron beam reflected through the interferometer contains less than 2% (as measured by a polarization analyzer behind the interferometer) mixture of the polarized beam with the opposite polarization.

A static spin flipper with $\mathbf{B} \approx B_{\mathrm{SF}}\hat{\mathbf{y}}$ is placed in the beam path between the prism field assembly and the interferometer to rotate the neutron polarization from

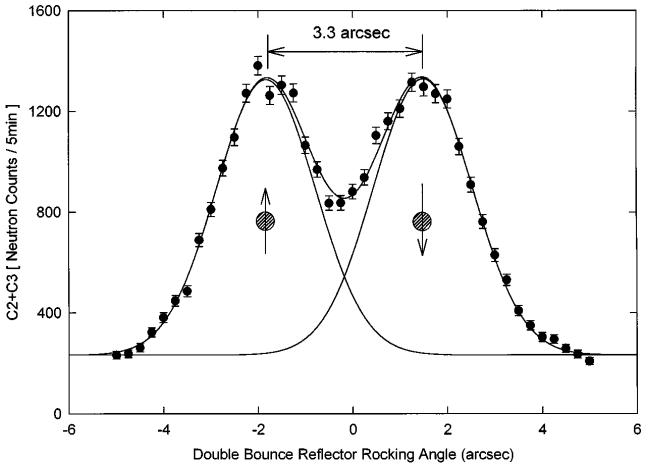

FIG. 2. Rocking curve of the double-bounce reflector against the interferometer, showing the birefringence splitting of 3.3 arcsec. The two neutron peaks have opposite polarization. The total intensity C2 + C3 is shown.

the vertical z direction to the longitudinal x direction. The flipper coil consists of 13 layers of anodized aluminum foil formed on a rectangular aluminum frame that is 12.5 mm along the beam path and 12.5 mm high. The longitudinally polarized neutron beam selected by the interferometer is split into two wave packets at the first silicon blade. An optically flat, 1 mm thick, aluminum plate is placed in one leg, producing a nuclear phase shift $\Delta\phi_{\rm nuc}$ which establishes the initial phase in the measurements. The wave packet in the other leg passes through the 44 mm long *pulse coil* solenoid whose field $\mathbf{B}(t) = B_{\rm pulse}(t)\hat{\mathbf{x}}$ is along the beam direction. At the last blade of the interferometer, the two wave packets are brought back together to mix and interfere. The interference results in intensity oscillations in the two outgoing beams as a function of the phase shift. In order to maintain the polarization of the neutrons, a uniform longitudinal 3 G guide field is established over the entire interferometer by an array of permanent magnets. Time-of-flight (TOF) electronics are connected to the two ^{3}He neutron detectors C2 and C3.

The polarization state *not* selected by the interferometer goes downstream onto the polarization analyzer, where it is reflected by the (111) reflection of a magnetically saturated $Co_{0.92}Fe_{0.08}$ crystal placed in an applied field in the $+z$ direction (perpendicular to the scattering plane). The analyzed beam is a mixture of both polarization states as the interferometer also transmits a fraction of its accepted state. At the analyzer, only the $+z$ spin component of the neutron beam is reflected. Using a dc current in the pulse coil causes an imperfectly (longitudinally) polarized (due to nonperfect spin flipping) neutron spin to precess, changing the relative $+z$ and $-z$ *amplitudes.* As a function of applied B-field strength, these amplitudes change and are measured in the reflected neutron intensity of the polarization analyzer. For a classical spin orientation other than longitudinal, this intensity variation is oscillatory with the B-field strength. However, in the case of a longitudinally polarized neutron beam (perfect spin flipping), the $+z$ and $-z$ amplitudes are *always* equal and the reflected intensity is independent of the dc B-field strength in the pulse coil. A series of scans for different spin-flipper field strengths and tilt angles have been carried out. Shown in Fig. 3 are representative plots of the polarization analyzer intensity as a function of the B-field strength for neutrons subjected to different fields in the spin flipper. The oscillatory neutron intensity variation disappears when the neutron beam is precisely longitudinally polarized.

To observe the SAB effect, a time-dependent pulsed magnetic field $\mathbf{B}(t) = B_{\rm pulse}(t)\hat{\mathbf{x}}$ is produced by applying a square pulse current sequence to the coil. The current pulse duty cycle is 128 μs, with two 8 μs pulses of opposite polarity separated by 64 μs every cycle. The phase shift acquired by any neutron along the beam path, $\Delta\Phi(x, v)$, is a convolution of the pulsed B-field profile

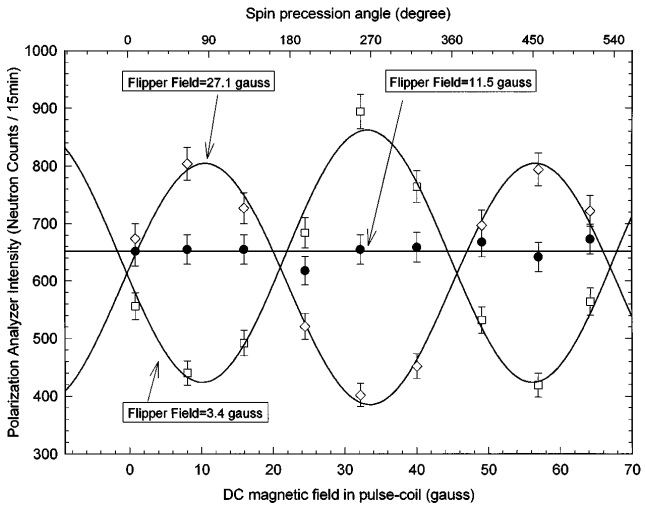

FIG. 3. Determining the classical neutron polarization: The technique is explained in the text. The amplitude of the oscillatory pattern is proportional to the angle the classical neutron polarization makes with an applied dc longitudinal B field in the pulse coil. The neutrons are polarized precisely longitudinally when this amplitude vanishes (filled circles).

$B_{\rm pulse}(t)$ with the pulse coil spatial field profile. The spatial dependence of this phase shift can be converted to a TOF scale by dividing the variable x by v, the neutron velocity. The time variable labels the arrival time of the neutrons at the detectors. The interferogram intensities in the detectors are each of the form

$$I(t, v) = A \pm C\cos[\Delta\phi_{\rm nuc} - \Delta\Phi(t, v)], \qquad (2)$$

The measurements were carried out with the nuclear phase $\Delta\phi_{\rm nuc} = \pi/2$ set by the aluminum phase plate. Although the SAB phase shift is nondispersive [7], the neutrons at the entrance and the exit of the pulse coil when the field is turned on do experience a spatial field gradient. Moreover, neutrons with different wavelengths starting at the same point along the beam path will not arrive at the detector at the same time because they have different speeds. The TOF intensity profiles at the detectors are, therefore, a convolution of the velocity profile associated with the wavelength distribution and the intensities given by Eq. (2). The velocity profile is sharply peaked about $v_0 = 1.68$ mm/μs with $\delta v/v_0 \sim 0.01$. Furthermore, the detection probability through the 12 mm diameter cylindrical ^{3}He detectors is also included to model the observed TOF pattern. The details of the pulse coil and the time-of-flight computations can be found in the papers by Allman *et al.* [5]. Multichannel scalars with channel advance every 2 μs are connected to the detectors to record the TOF pattern. Figure 4 contains a set of the measured TOF patterns for different pulsed B-field strengths. The phase shift dependence is revealed as changes of the peak amplitude. The solid lines are predictions from model computations explained above.

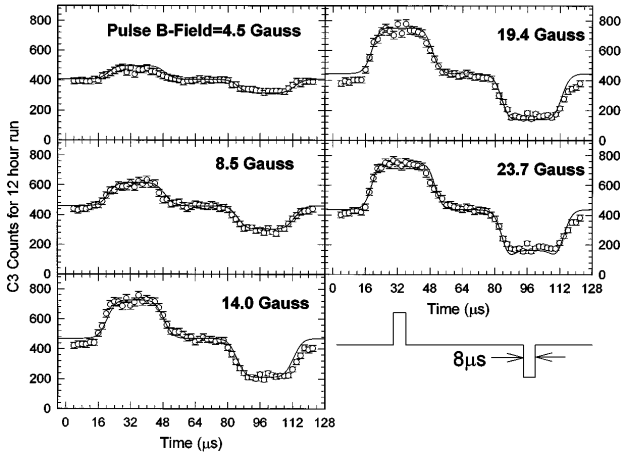

FIG. 4. A set of TOF neutron intensity patterns for increasing pulsed field strength. The average counting rate in the middle of the positive and negative field pulses is used to obtain the SAB interference plotted in Fig. 5. The solid lines are the results of theoretical model fits to the data as explained in the text.

Of special interest is the case in which the neutrons travel inside the uniform magnetic field region for the duration of the magnetic field pulse. The magnetic field generated by the pulse coil is uniform to within 1% over 28 mm of its length. For the 1.68 mm/μs velocity of the 2.35 Å neutrons, a 14 mm long column of neutrons experiences a spatially uniform field for 8 μs and acquire only the SAB phase shift, namely,

$$\Delta\Phi_{\mathrm{AB}} = \frac{1}{\hbar}\int_{\Delta T} \mu B_{\mathrm{pulse}}(t)\, dt\,. \qquad (3)$$

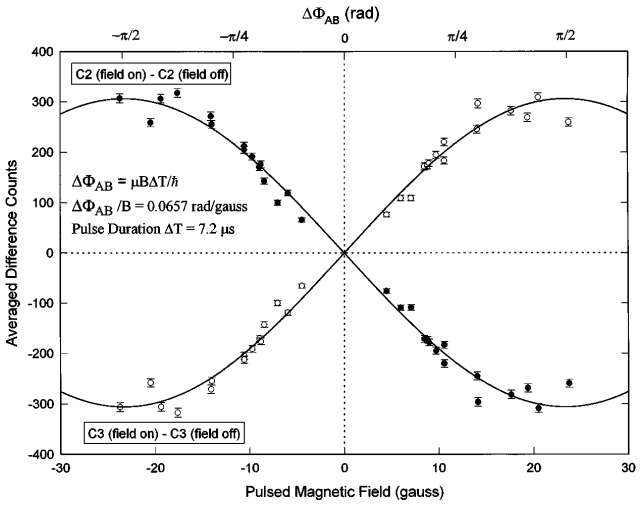

FIG. 5. SAB interference intensity, shown as difference counts of positive and negative field pulses relative to the zero-field counts, plotted as a function of the pulsed *B*-field strength. Each point is an average of four points at the center of the peak plateaus in the TOF patterns (Fig. 4). The solid lines are fits of a sinusoid to the data, with the pulse duration ΔT as the adjustable parameter.

This 8 μs time slice of data is located at the center of the peak plateaus in the interference TOF patterns. A plot of the average of difference counts (relative to the zero-field counts) for both the positive and negative field pulses as a function of the pulsed *B*-field strength (lower horizontal axis) and the phase shift (upper horizontal axis) is shown in Fig. 5. The zero-field intensity is subtracted from the data to obtain the amplitude related to the B field. The sinusoidal interference pattern is clearly evident. Fitting the data to the SAB formulas yields an effective pulse time of 7.2 μs, in reasonable agreement with the expected 8 μs pulse time. Since there is neither a classical force nor a classical torque on these neutrons, the interference can be explained only by the quantum mechanical SAB effect, having no classical manifestation or interpretation.

This work was supported by NSF Physics Division, Grant No. 9603559. B. E. A. acknowledges support from an Australian Research Council grant during the writing of this paper.

[1] Y. Aharonov and D. Bohm, Phys. Rev. **115**, 485 (1959); for a comprehensive review, see M. Peshkin and A. Tonomura, *The Aharonov-Bohm Effect*, Lecture Notes in Physics Vol. 3450 (Springer-Verlag, Berlin, 1989).

[2] G. Mateucci and G. Pozzi, Phys. Rev. Lett. **54**, 2469 (1985).

[3] A. Zeilinger, in *Fundamental Aspects of Quantum Theory*, NATO ASI, Ser. B Vol. 144, edited by V. Sorini and A. Frigerio (Plenum, New York, 1985).

[4] J. Anandan, Phys. Lett. A **138**, 347 (1989); **152**, 504 (1991); in *Proceedings of the 3rd International Symposium on the Foundations of Quantum Mechanics, Tokyo, 1989* (Physical Society of Japan, Tokyo, 1990), pp. 98–106.

[5] B. E. Allman, A. Cimmino, A. G. Klein, G. I. Opat, H. Kaiser, and S. A. Werner, Phys. Rev. Lett. **68**, 2409 (1992); Phys. Rev. A **48**, 1799 (1993).

[6] M. Peshkin, Phys. Rev. Lett. **69**, 2017 (1992); M. Peshkin and H. J. Lipkin, Phys. Rev. Lett. **74**, 2847 (1995); P. Pfeifer, Phys. Rev. Lett. **72**, 305 (1994); **70**, 3365 (1993). Peshkin and Lipkin conclude that the SAB phase shift experiment of Allman *et al.* (Ref. [5]) is not topological in the usual context of the gauge fields *V* and **A** entering the AB effects for electrons. Pfeifer reaches the opposite conclusion and emphasizes the nondispersive character ($\partial\Delta\Phi_{\mathrm{AB}}/\partial k = 0$) of all AB effects (see also Refs. [3,7]).

[7] G. Badurek, H. Weinfurter, R. Gähler, A. Kollman, S. Wehinger, and A. Zeilinger, Phys. Rev. Lett. **71**, 307 (1993).

[8] W.-T. Lee, O. Motrunich, B. E. Allman, and S. A. Werner, in *Proceedings of the International Symposium on Neutron Optics and Related Research Facilities, Kumatori, 1996* [J. Phys. Soc. Jpn. **65**, Suppl. A, 210 (1996)].

[9] R. Clothier, H. Kaiser, S. A. Werner, H. Rauch, and H. Wolwitsch, Phys. Rev. A **44**, 5357 (1991).